inter.noise
HAMBURG 2016

An investigation of the influence of wheel/rail contact conditions on curve squeal

Stefano ALFI[1]; Simone BARO[2]; Roberto CORRADI[3];
Giacomo SQUICCIARINI[4]; David J. THOMPSON[5]; Matthias ASPLUND[6]

[1, 2, 3] Politecnico di Milano - Department of Mechanical Engineering, Italy

[4, 5] ISVR - University of Southampton, UK

[6] Trafikverket - Swedish Transport Administration, Sweden

ABSTRACT

In this paper the influence of wheel/rail contact conditions on the possible occurrence of curve squeal is investigated. A reference case is presented, together with the available experimental data, and the results of numerical simulations are illustrated. The analyses reported in the paper are based on two calculation steps. First 3D multibody simulation of a rail vehicle running in curve is carried out. Then squeal simulation is performed, which is based on linear wheel and rail dynamic models, coupled through a nonlinear contact model. Stability analysis of the open loop transfer function of the overall system yields the possible unstable frequencies.

Keywords: Curve Squeal, Wheel/Rail Contact, Vehicle Multibody Simulation, Squeal Simulation

1. INTRODUCTION

Curve squeal is produced by the self-excited vibration of a railway wheel, as a result of the contact phenomena taking place at wheel/rail interface during curve negotiation (1). Squeal noise is thought to be mainly caused by unsteady lateral creepage (1,2) while other mechanisms, like wheel flange rubbing and differential slip between the wheels on the same axle, has been demonstrated to be of secondary importance (3,4). Curve squeal has been widely investigated by means of experimental tests and analytical/numerical models (1-9). Parametric studies (5-7) have shown that, in addition to the angle of attack and the friction coefficient, squeal occurrence depends on the lateral wheelset position as well as on the geometry of the coupled wheel/rail profiles since both affect the local contact conditions. Most squeal models follow the approach adopted by Rudd (2), introducing a negative slope of the friction characteristic (i.e. a weakening of the friction coefficient with increasing sliding velocity) as the source of instability (5,8,9). However, unstable vibration may also arise from friction-induced mode coupling, which results in flutter instability (6). Both falling friction and friction-induced flutter probably coexist as possible instability mechanisms and need to be taken into account together to justify curve squeal occurrence under different contact conditions.

The present work, carried out in the frame of the European Project In2Rail, aims at investigating the influence of wheel/rail contact on the possible occurrence of squeal noise. The analyses are based on the combination of two numerical models, corresponding to two simulation steps carried out in sequence.

For a given vehicle, during negotiation of a curve, the steady-state distribution of the contact forces over the four wheels within a bogie varies not only with the curve geometry (radius and cant) and the train speed, but also with the friction coefficient and the geometry of the coupled wheel/rail profiles. This paper addresses the problem of estimating the influence of these parameters on the forces

[1] stefano.alfi@polimi.it
[2] simone.baro@polimi.it
[3] roberto.corradi@polimi.it
[4] g.squicciarini@soton.ac.uk
[5] djt@isvr.soton.ac.uk
[6] matthias.asplund@trafikverket.se

exchanged at wheel/rail interface and on the consequent possible occurrence of curve squeal. Attention is focused on the inner wheel of the third axle of the reference train.

2. REFERENCE CASE

The reference case considered in this paper is a left-hand curve in the Stockholm commuter rail network, with 300 m radius and 0.14 m cant. The rolling stock running on consists of multiple-unit electric trains, with 6 car bodies and 7 bogies (2 traditional end bogies with 2.4 m wheelbase and 5 Jacobs-type bogies with 2.7 m wheelbase in the middle). The average axle load is approximately 150 kN.

Trackside sound pressure measurements taken on this reference curve allow the dominant frequencies involved in curve squeal to be identified. Figure 1 shows the spectrogram and the SPL spectrum over a whole pass by. Above 4 kHz there are at least five sharp peaks. The first three are centred at 4870, 5870 and 6580 Hz. Since these measurements are from a microphone located at a fixed position, the data include contributions of the noise radiated by all the wheels.

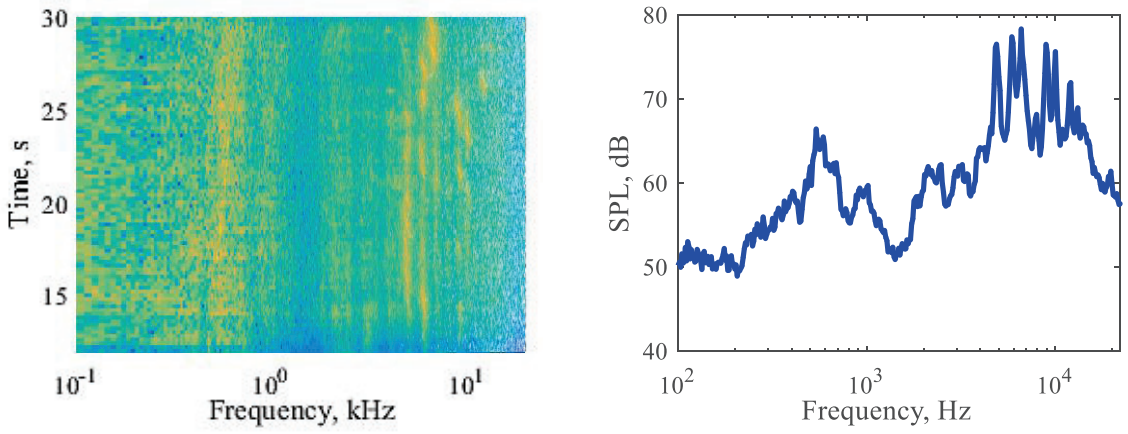

(a) (b)

Figure 1 - Trackside noise measurements (300 m radius curve negotiated at 60 km/h).

(a) Spectrogram and (b) SPL spectrum (L_{eq} for pass-by)

An axisymmetric finite element (FE) model of the wheel was developed in ANSYS for use in the squeal simulations described in section 3. Wheel receptances are calculated by modal superposition; a damping ratio of 10^{-4} is given to all the modes having two nodal diameters or more. The resulting receptances in axial and radial directions at the nominal contact point are shown in Figure 2.

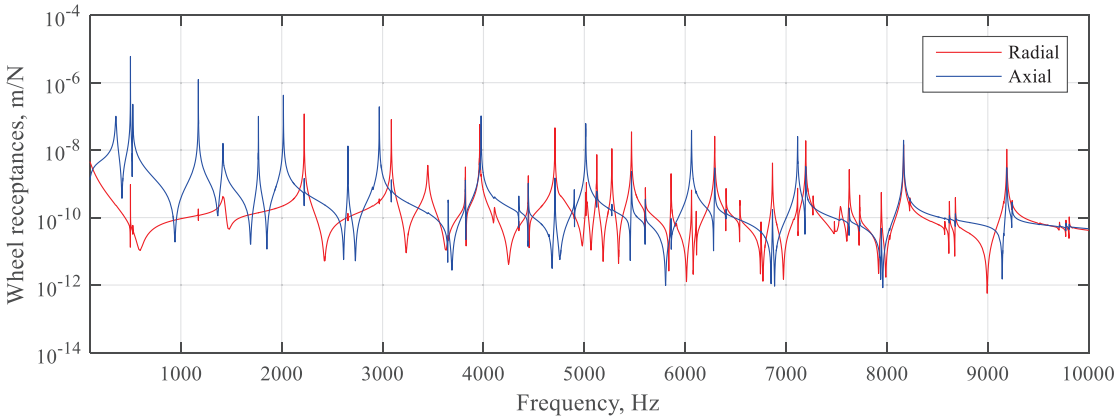

Figure 2 - Wheel receptances at the nominal contact point (FEA)

The computed natural frequencies of the wheel modes that could be contributing to squeal (Figure 1) are listed in Table 1. The vibration modes in Table 1 correspond to the nominal wheel geometry. However the actual wear condition of the wheel during measurements is not known and the natural frequencies of the worn wheel are expected to differ from those of the new wheel.

Table 1 - Wheel modes (FEA)

Mode type *number of nodal diameters number of nodal circles R for radial modes*	***Natural frequency (Hz)***	***Mode shape***
(5,R)	4708	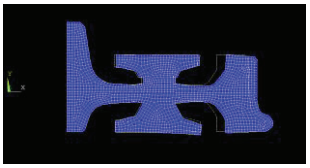
(7,0)	5013	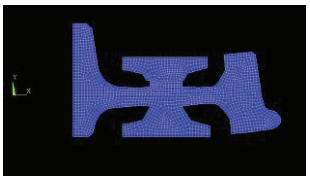
(6,R)	5468	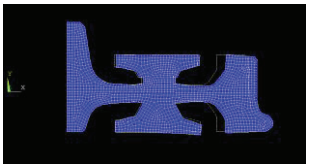
(8,0)	6063	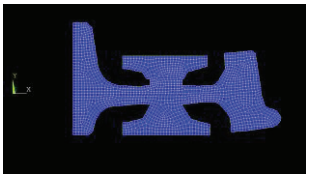
(7,R)	6293	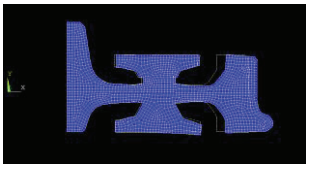
(9,0)	7114	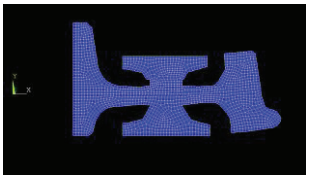

3. NUMERICAL SIMULATION APPROACH

The analyses presented in this paper are based on two simulation steps. First 3D multibody simulation of a rail vehicle running in curve is carried out, and then squeal simulation is performed in frequency domain. This is based on linear wheel and rail models, coupled through a linearized contact model.

Multibody simulations are executed by means of a software developed at Politecnico di Milano (10-12) that allows the dynamic behaviour of a rail vehicle running in tangent and curved track to be simulated. Large displacements and consequent kinematic nonlinearities are considered.

The wheel/rail contact model implemented in the multibody simulation can account for multiple contact points on the same wheel (this is the typical situation that occurs on a flanging wheel). The normal forces are evaluated through a multi-Hertzian model (13) which allows either to include the presence of multiple contacts or to approximate complex non-Hertzian contact patches by one or more

elliptic patches. The transverse and longitudinal contact forces are then determined through the heuristic Shen-Hedrick-Elkins contact model (14), starting from the transverse and longitudinal creepages in each contact area, which are derived from the wheelset kinematics.

As a result of the multibody simulation, the steady-state values during negotiation of a curve of the following quantities are computed for the generic wheel, and given as input to the squeal calculation:

- angle of attack;
- position of each contact point across the wheel profile;
- normal contact force on each contact patch;
- transverse, longitudinal and spin creepages on each contact patch.

The second simulation step (squeal model) is based on a linear description of the wheel and rail dynamics while the non-linear representation of friction coefficients as a function of creepages proposed by Kraft (15) is adopted to calculate the contact forces. To establish the possible unstable modes, the contact model is linearized around the steady-state curving condition obtained from multibody simulations.

The wheel is represented by means of its modal basis to give the mobilities at the nominal contact point (Figure 2); mobilities at the actual contact point are obtained by rigid translation and rotation of the mode shapes. Existing theoretical models are adopted to describe the rail mobilities (16). The relationship between friction coefficients and creepages is defined according to the FASTSIM algorithm (17). To introduce the falling region, a heuristic correction formula (15,16) is adopted of the form:

$$\left(1-\lambda\ e^{-\kappa/\gamma_{tot}}\right) \tag{1}$$

Where κ is determined for each case by evaluating the value of creepage at saturation of the contact patch from the multibody model, λ is taken as 0.65 and γ_{tot} combines the contribution of all creepages.

The simulations determine possible unstable eigenvalues of the wheel/rail system, through a stability analysis of the open loop transfer function of the overall system. Generally unstable frequencies coincide with (or are very close to) the natural frequencies of the wheel modes. The curve squeal model includes two possible sources of instability. The first is due to the negative slope of the friction curve above a certain creepage value (falling region). The other is the instability due to the coupling between two (or more) wheel modes. A more detailed description of the squeal model can be found in (9).

4. RESULTS

Three different scenarios are considered in the multibody simulations and in the following squeal noise analyses. The first simulation (Case 1) corresponds to the reference case reported in Section 2 where a train speed of 60 km/h and a friction coefficient of 0.35 are considered. Starting from this case, a second multibody simulation is performed (Case 2) to investigate the influence of the friction coefficient. In this simulation the friction coefficient is set to 0.6. Furthermore, the effect of the vehicle speed is taken into account in a third simulation (Case 3), increasing it to a value of 86 km/h and maintaining the same friction coefficient of the reference case. The input parameters for the three multibody simulations are summarized in Table 2.

Table 2 - Input parameters for the three performed multibody simulations

Parameters	***Case 1***	***Case 2***	***Case 3***
Curve direction	Left	Left	Left
Curve radius (m)	300	300	300
Cant (m)	0.14	0.14	0.14
Vehicle speed (km/h)	60	60	86
Friction coefficient	0.35	0.6	0.35

An example of multibody simulation results for the reference case (Case 1) is shown in Figure 3. The figure shows the contact force distribution on the wheels of the third axle of the vehicle in full curving. For a standard railway vehicle, the first wheelset is normally selected, when investigating

squeal noise. However, for the particular type of vehicle considered in this study, the focus is on the third axle, which exhibits worse curving conditions due to the longer wheelbase of the second bogie (2.7 m) with respect to the first one (2.4 m). In steady-state conditions, there is only one contact point located on the tread on the inner (left) wheel whereas the outer (right) wheel shows two contact points, one located at the flange root and a second one on the flange. A high value of normal contact force on the inner wheel can be observed. This is due to the small value of cant deficiency in the curve. According to the reference condition, at 60 km/h and with a rail cant of 0.14 m, the vehicle negotiates the curve in an almost perfectly compensated condition, thus resulting in negligible load transfer between the inner and outer wheel (the overall vertical force is 69.5kN on the outer wheel and 72.5kN on the inner one).

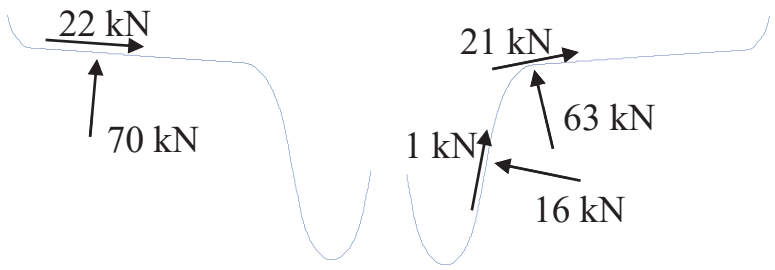

Longitudinal contact forces (kN) (positive in forward direction)		
Left wheel	Tread	-11
Right wheel	Root flange	5.5
	Flange	5.5

Figure 3 - Multibody simulation of the reference case (Case 1): contact forces on the wheels of the 3rd axle.

The same type of contact point distribution and position is found for Cases 2 and 3, which are not reported here for the sake of brevity.

Table 3 summarizes, for the three scenarios considered, the output data obtained from the multibody simulations that form the input to the squeal noise analyses. In this study, the squeal analysis investigates only the inner wheel; therefore the data in Table 3 represent the contact conditions of only the contact point on the inner wheel of the third axle. In Table 3, the sign conventions refer to a local contact reference frame with positive longitudinal axis in the forward direction (L), positive transverse axis towards the left (T) and a vertical axis forming a right-handed reference system so that it is positive in the direction entering the wheel (N). Longitudinal and transverse creepages are positive according to the axes directions and spin creepage is positive for a positive rotation around the vertical axis.

Table 3 - Steady-state values for the 3rd axle inner wheel parameters given as input to the squeal simulation

Parameters	***Units***	***Description***	***Case 1***	***Case 2***	***Case 3***
σ	mrad	Angle of attack	8.7	7.9	7.4
θ	deg	Contact angle	-1.0	-1.0	-1.0
N	kN	Normal contact force	69.7	71.9	36.7
γ_L	-	Longitudinal creepage	0.0045	0.0057	0.0058
γ_T	-	Transverse creepage	0.0087	0.0079	0.0074
γ_{SN}	1/m	Spin creepage	-0.0355	-0.0356	-0.0355

From Table 3, it is important to observe that in Case 1 there is a high value of transverse creepage, 0.0087, due to the high angle of attack (for steady-state contact on the tread, the transverse creepage is almost equal to the angle of attack) and that the saturation of the contact patch is in the transverse direction (the ratio between transverse and longitudinal creepages is 1.95). Passing from Case 1 to Case 2, it can be seen that the friction coefficient increases, from 0.35 to 0.60, causing a reduction of the transverse creepage to 0.0079 (due to a corresponding reduction of the angle of attack) together with an increase of the longitudinal creepage that therefore reduces the saturation in the transverse direction (the ratio between transverse and longitudinal creepages becomes 1.37). In the same way, comparing Case 1 and Case 3, the effect of the speed increase is again to reduce the transverse

creepage (0.0074) and to increase the longitudinal one (the ratio becomes 1.26). The main difference between Case 2 and 3 is given by the normal contact force that is almost halved in Case 3 with respect to Case 2. This effect is related to the different cant deficiency: while in Case 1 and 2 the vehicle negotiates the curve with almost zero cant, in Case 3 the cant deficiency is equal to 150 mm (1 m/s^2 non-compensated lateral acceleration) causing a substantial load transfer towards the outer wheel.

To evaluate the effect of these curving conditions on curve squeal, data from Table 3 are used as nominal values for a Monte Carlo analysis in the squeal simulations. Input data is given a uniform distribution centered at the nominal value and having a range as summarized in Table 4. For each case 50 different calculations are performed, each of them defined by randomly extracting a single value from the uniform distributions.

Table 4 - Input parameters for curve squeal model

Parameter	***Units***	***Description***	***Range of values***
N_0	kN	Normal force	$N_0 \pm 5\%$
V_0	m/s	Speed	$V_0 \pm 5\%$
κ	-	Eq. (1)	$\kappa_0 \pm 5\%$
λ	-	Eq. (1)	0.65
θ	deg	Contact angle	$\theta_0 \pm 0.5°$
γ_L	-	Longitudinal creepage	$\gamma_{L_0} \pm 10\%$
γ_T	-	Transversal creepage	$\gamma_T \pm 10\%$
γ_{sN1}	1/m	Spin Creepage	$\gamma_{SN,0} \pm 10\%$
P	mm	Contact point	$[0 \quad y_{T0} \pm 5 \quad 0]$

Steady-state creepages and friction curve ranges for each of the three cases are shown in Figure 4. For the first case (Figure 4(a)) steady state creepages are in the falling friction region therefore more likely to result in curve squeal. For this case saturation of the contact patch is found for a transverse creepage of 0.007. In the second case (Figure 4(b)) the increased friction coefficient causes a reduction of steady-state transverse creepage and at the same time an increase in the value of creepage at which saturation of the contact patch occurs. Both effects are beneficial in minimizing curve squeal; in fact the set of input data for this second case do not lie in the falling region. Finally in Case 3 the increased speed again results in lower steady state creepages and in an increased longitudinal creepage. Both have a positive effect on curve squeal; input data are moved into a region where the falling region is less severe than in Case 1 (Figure 4(c)).

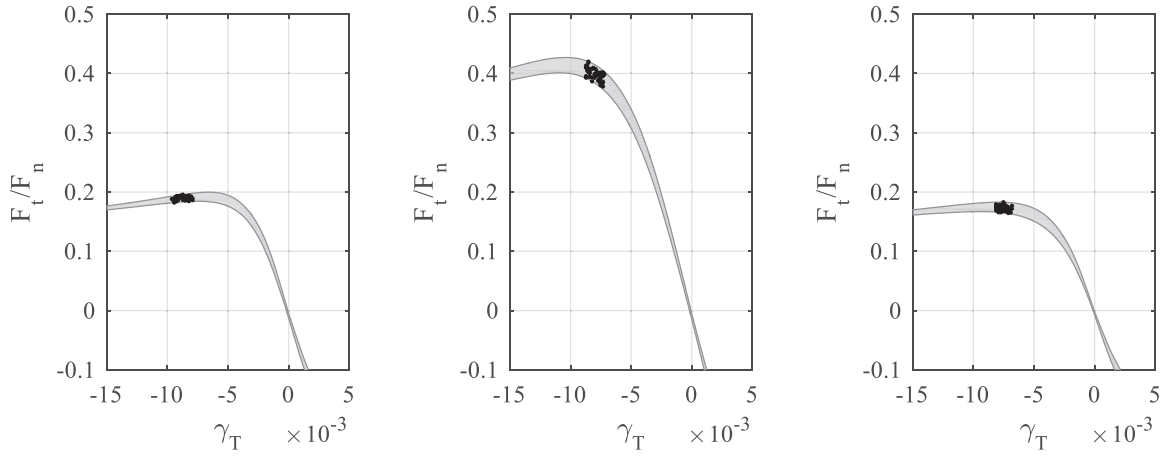

Figure 4 - Normalized lateral creep force as function of lateral creepage. Grey area: range of variability for friction curve, (·): steady state creepage for each case. (a) $\mu_0 = 0.35$ and $V = 60$ km/h; (b) $\mu_0 = 0.35$ and $V = 86$ km/h and (c) $\mu_0 = 0.6$ and $V = 60$ km/h.

In terms of curve squeal predictions the model gives, for any given run, a series of possible unstable eigenvalues. This result is summarized in Figure 5 for Case 1 where each black dot corresponds to an unstable eigenvalue for one of the model runs arranged vertically. In the background the figure also displays the wheel mobility at the nominal contact point. From this it can be inferred that most of the axial modes could contribute to curve squeal in this condition. Although this calculation shows that modes below 2 kHz seem to be more likely to give curve squeal, also modes above 5 kHz can result in self-excited vibration. A time-domain simulation could give more insight into which are the actual modes that would develop squeal.

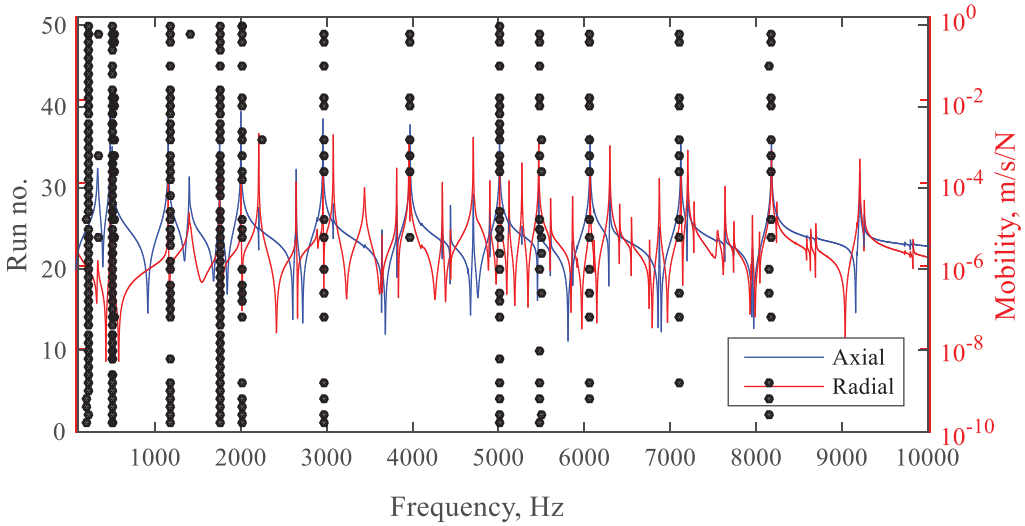

Figure 5 - Curve squeal occurrences for $\mu_0 = 0.35$ and $V = 60$ km/h.

From the predictions for Case 2, curve squeal did not appear for any of the modes above 300 Hz, while in Case 3, out of the 50 simulations, curve squeal developed only once. The unstable eigenvalue was found at 500 Hz.

It is quite intuitive to understand that increased speed can have a positive effect on curve squeal: an increase in speed decreases the angle of attack and therefore decreases transverse creepage. Case 2 is less intuitive as calculations show that increased friction coefficient can strongly decrease the likelihood of curve squeal. The simulations show that an increased friction coefficient reduces the angle of attack (and transverse creepage) as well as moving the creepage value at which saturation of the contact patch occurs toward higher (in magnitude) values.

The range chosen for the simulations is arbitrary as is the friction curve. This procedure (9), however, introduces the effect of uncertainty on input parameters on curve squeal prediction. Certainly a wider range in the initial distribution of data could result in a different set of predictions. It is expected, however, that these simulations capture the correct trend.

5. CONCLUSIONS

This paper showed a possible approach to investigate the effect of contact conditions on curve squeal. Input data from a multibody simulation of a curving train were given as input to a curve squeal model in the frequency domain. Focusing on the inner wheel, by changing the friction coefficient and train speed it was possible to study how differences in curve negotiation can affect curve squeal. In particular it was found that for a lower friction coefficient (0.35) and nominal curving conditions, the likelihood of curve squeal is high. On the other hand, for the scenario considered, by either increasing the friction coefficient (to 0.6) or by increasing the train speed from 60 to 86 km/h, the occurrences of curve squeal can decrease or disappear.

6. ACKNOWLEDGEMENTS

The work described has been supported by the EU under the collaborative project ‘In2Rail’.

REFERENCES

1. Thompson D.J. Railway Noise and Vibration, Elsevier Science, (2008).
2. Rudd M.J. Wheel/rail noise - Part II: wheel squeal. Journal of Sound and Vibration, 46 (3), 395-417, (1976).
3. Vincent N., Koch J.R., Chollet H., Guerder J.Y. Curve squeal of urban rolling stock – Part 1: State-of-the-art and field measurements. Journal of Sound and Vibration, 293 (3-5), 691-700, (2006).
4. Koch J.R., Vincent N., Chollet H., Chiello O. Curve squeal of urban rolling stock – Part 2: Parameter study on a 1/4 scale rig. Journal of Sound and Vibration, 293 (3-5), 701-709, (2006).
5. De Beer F.G., Janssens M.H.A., Kooijman P.P. Squeal noise of rail-bound vehicles influenced by lateral contact position. Journal of Sound and Vibration, 267 (3), 497-507, (2003).
6. Pieringer A. A numerical investigation of curve squeal in the case of constant wheel/rail friction. Journal of Sound and Vibration, 333 (18), 4295-4313, (2014).
7. Glocker Ch., Cataldi-Spinola E., Leine R.I. Curve squealing of trains: Measurement, modelling and simulation. Journal of Sound and Vibration, 324 (1-2), 365-386, (2009).
8. Chiello O., Ayasse J.B., Vincent N., Koch J.R. Curve squeal of urban rolling stock – Part 3: Theoretical model. Journal of Sound and Vibration, 293 (3-5), 710-727, (2006).
9. Squicciarini G., Usberti S., Thompson D.J., Corradi R., Barbera A. Curve squeal in the presence of two wheel/rail contact points. Notes on Numerical Fluid Mechanics and Multidisciplinary Design, 126, 603-610, (2015).
10. Bruni S., Collina A., Diana G., Vanolo P. Lateral dynamics of a railway vehicle in tangent track and curve: tests and simulation. Vehicle System Dynamics, 33 (SUPPL.), 464-477, (2000).
11. Alfi S., Bruni S. Mathematical modelling of train-turnout interaction. Vehicle System Dynamics, 47 (5), 551-574, (2009).
12. Cheli F., Corradi R., Diana G., Facchinetti A. Validation of a numerical model for the simulation of tramcar vehicle dynamics by means of comparison with experimental data. Journal of Computational and Nonlinear Dynamics, 2 (4),.299-307, (2007).
13. Pascal J.P., Savage G. Available methods to calculate the wheel/rail forces in non-hertzian contact patches and rail damaging. Vehicle System Dynamics, 22 (3-4), 263-275, (1993).
14. Shen Z.Y., Hedrick J.K., Elkins J.A. Comparison of alternative creep-force models for rail vehicle dynamic analysis. Dynamics of Vehicles on Roads and Tracks, Proceeding of the 8th IAVSD Symposium, 591-605, (1984).
15. Kraft K. Der Einfluß der Fahrgeschwindigkeit auf den Haftwert zwischen Rad und Schiene. AET 22 Addendum to ETR, 58–78, (1967).
16. Huang Z. Theoretical Modelling of Railway Curve Squeal. PhD Thesis, University of Southampton, Institute of Sound and Vibration Research, (2007).
17. Kalker J.J. A Fast Algorithm for the Simplified Theory of Rolling Contact. Vehicle System Dynamics, 11 (1), 1-13, (1982).